Progress In Electromagnetics Research, Vol. 139, 799–819, 2013

ULTRASENSITIVE SWITCHING BETWEEN RESONANT REFLECTION AND ABSORPTION IN PERIODIC GRATINGS

Nikolay Komarevskiy*, Valery Shklover, Leonid Braginsky, and Christian Hafner

Swiss Federal Institute of Technology (ETH) Zürich, Zürich 8092, Switzerland

Abstract—Guided-Mode Resonance (GMR) effects in transparent periodic gratings possess a number of remarkable phenomena. GMRs exhibit strong features in the optical spectrum, i.e., dips, peaks, cusps, and may attain extremely high Q-factors. In some cases, resonant reflection with the efficiency equal to unity can be observed. We demonstrate that the introduction of small losses in the structure can drastically modify its optical response by causing strong absorption resonances. Unity reflection in loss-free structures can be almost completely converted into unity absorption peaks as soon as very small losses are introduced. Even thin absorbing films in the structure (or in its vicinity) can lead to such strong resonant absorption effects. The resonances may exhibit a negligible spectral shift, but a significant variation in the magnitude when losses are slightly altered, which is highly attractive for sensor and switch applications. Absorption peaks experience a resonant behavior with respect to both frequency and material losses. We show that the width of the absorption peaks decreases and approaches the width of the reflection peaks, as losses decrease. Thus, high-Q resonances can be observed. The absorption resonances also possess strong angular dependence; they may split and significantly increase in magnitude for a slightly inclined incidence. We elucidate the resonant reflection/absorption effects theoretically and provide numerical examples.

1. INTRODUCTION

In transparent periodic dielectric gratings, a resonant reflection with the theoretical efficiency equal to unity can be achieved, due to the

Received 17 April 2013, Accepted 16 May 2013, Scheduled 26 May 2013

* Corresponding author: Nikolay Komarevskiy (n.komarevskiy@ifh.ee.ethz.ch).

excitation of leaky modes [1]. The experimental realization of such high-efficiency Guided-Mode Resonance (GMR) filters was reported in [2, 3]. Underlying physics of the strong GMRs with very high Q-factors was explained in [4]. Energies, linewidths and field distribution of leaky (or quasiguided) modes were calculated in [5]. Such GMR structures are used as sensors for biochemistry [6, 7], humidity [8], pressure [9], angle measurements [10] and may be used for other applications as well [11]. The sensing scheme employs a light source, an optically transparent periodic grating (which supports guided-mode resonances) and an optical detector, see Fig. 1. The sensing principle utilizes the idea, that the change in the structure geometry or in the real part of the dielectric permittivity ε' of the media, causes a resonance shift, that can be optically detected.

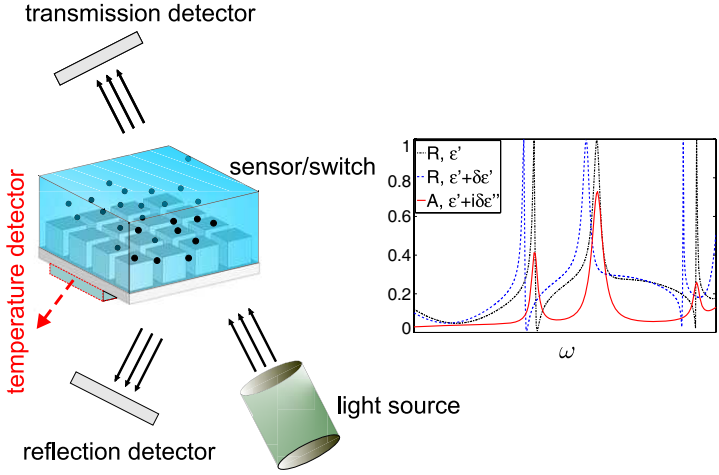

Figure 1. The scheme of a conventional GMR sensor, which comprises a light source; a dielectric grating, which supports at least one guided-mode resonance; an optical detector, working in reflection or transmission mode. The change in the real part of permittivity by $\delta\varepsilon'$ causes resonance shift, shown on the right (blue and black curves). Introduction of small losses $\delta\varepsilon''$ manifests in strong absorption peaks (red curve).

To the best of our knowledge, the influence of the imaginary part of the permittivity ε'' (i.e., the material losses) on the GMR performance has not been considered [12]. Our simulations reveal that absorption effects caused by losses may be even stronger than the resonance shifts, caused by the change of the real part of the permittivity ε'. Small losses can lead to a huge increase of the absorption at resonance, as

shown by red curve in Fig. 1. We call this phenomenon Absorption-Based Guided-Mode Resonance (AGMR). The sensitivity to the loss term can be extremely high. In some cases, total reflection can almost completely be turned into total absorption or consequently into heat. Therefore, two substantial benefits for utilizing AGMR in sensor and switch applications are: potentially higher sensitivity and a simplified readout scheme. For example, one can employ a simple temperature measurement of the structure, rather than a spectral measurement of the resonance shift, see Fig. 1.

The paper is organized as follows. In Section 2, we consider a simple model, which allows analytical evaluation of the resonant reflection/absorption. It is shown that even small material losses, cause absorption resonances. The angular dependence of the absorption resonances is analyzed. It is shown that the resonances may be extremely sensitive with respect to the angle of incidence. In Section 3, we consider three-dimensional structures with resonant reflection and absorption effects and analyze the position and line widths of the resonances. For a specific structure we demonstrate that the introduction of small losses can almost completely convert unity reflection into unity absorption. In Section 4, we show that material losses are not required to be present throughout the structure for obtaining resonant absorption effects. Even very thin layers in the AGMR structure (or in its vicinity) can cause resonant absorption effects. As an example, we introduce a conducting graphene monolayer in a loss-free structure and obtain strong absorption resonances. Finally, in Section 5 the angular dependence of the resonances for three-dimensional structures is studied. In the Appendix, we demonstrate that the linewidths of the absorption peaks for small losses approach those of the resonant reflection for the loss-free case.

2. RESONANT REFLECTION AND RESONANT ABSORPTION

To understand the phenomenon, let us consider the light reflection from a dielectric slab with a periodic boundary on the top (see Fig. 2). Assume that the dielectric permittivity at the upper interface has the form:

$$\begin{aligned} \varepsilon(x,z) &= \varepsilon_1 + (\varepsilon_2 - \varepsilon_1)\theta(z) + 2\gamma\delta(z)\cos Gx, \\ \theta(z) &= \begin{cases} 0, & z<0 \\ 1, & z\geq 0 \end{cases} \qquad \delta(z) = \begin{cases} \infty, & z=0 \\ 0, & z\neq 0 \end{cases} \end{aligned} \tag{1}$$

where $\theta(z)$ and $\delta(z)$ are Heaviside step and Dirac delta functions, $G = 2\pi/d$, where d is the period of the perturbed interface. The

interface described by (1) is a physical model, corresponding to an interface modulated with respect to x-axis, but of zero thickness. The permittivities of the materials are $\varepsilon_1 = 1$ and $\varepsilon_2 = \varepsilon' + i\varepsilon''$, real part $\varepsilon' = 4$ shall be fixed, while ε'' is a variable parameter. The permeability is $\mu = 1$ for both media.

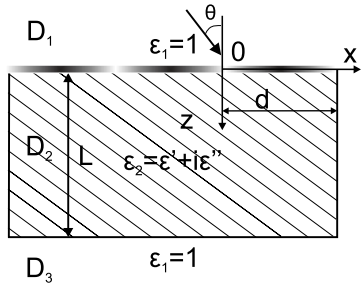

Figure 2. Dielectric grating with a sinusoidal $\varepsilon(x)$ interface at top. Permittivities are $\varepsilon_1 = 1$ and $\varepsilon_2 = \varepsilon' + i\varepsilon''$, $\varepsilon' = 4$. Thickness and period of the grating are $L = d = 100\,\text{nm}$. Light impinges on the structure at angle θ.

For a thin interface the scattering problem can be considered in terms of the boundary conditions for the electric (or magnetic) field of the light. Assume the electric field of the incident wave to be polarized in the y direction. The boundary conditions for the electric field $\mathbf{E} = (0, E(x,z), 0)$ can be obtained after integrating the wave equation over some narrow region at the boundary $z = 0$:

$$\frac{\partial^2 E}{\partial x^2} + \frac{\partial^2 E}{\partial z^2} + k_0^2 \varepsilon(x,z) E = 0, \tag{2}$$

where $k_0 = \omega/c$, ω is the frequency of light, c is the speed of light in vacuum. Thus, we find

$$[E] = 0, \qquad \left[\frac{\partial E}{\partial z}\right] + 2k_0^2 \gamma E(x) \cos Gx = 0. \tag{3}$$

Square brackets denote the discontinuity of the corresponding value at the boundary. To obtain the first equation of (3), we multiplied (2) by z before the integration by parts. The first boundary condition of (3) assumes continuity of the tangential component of the electric field. The second one is the generalization of the boundary condition for the tangential component of the magnetic field.

The electric field $E(x)$ at the periodic boundary can be represented as:

$$E(x) = \sum_n E_n e^{iG_n x}.$$

Thus, boundary conditions for the coefficients E_n of the n-th band are:

$$[E_n] = 0, \qquad \left[\frac{\partial E_n}{\partial z}\right] + k_0^2\gamma(E_{n+1} + E_{n-1}) = 0. \tag{4}$$

Equation (4) is the particular case of the boundary conditions for the envelope functions of the light waves proposed in [13]. We see that diffraction can also be interpreted as a band mixing at the interface. The simple cosine boundary of (1) results in the mixing of adjacent bands. In general, however, a periodicity of the boundary results in the mixing of many bands. The amount of mixing is proportional to the Fourier component of the dielectric permittivity at the boundary.

To consider light reflection from a dielectric grating, let us represent the electric field $E^{(m)}(x,z)$ in the domain D_m:

$$\sum_n A_n^{(m)+} \exp\left(i\alpha_n x + i\beta_n^{(m)} z\right) + \sum_n A_n^{(m)-} \exp\left(i\alpha_n x - i\beta_n^{(m)} z\right), \tag{5}$$

where

$$\alpha_n = k_x + Gn, \quad k_x = k_0 \sin\theta, \tag{6}$$

$$\beta_n^{(m)} = \left(\varepsilon_m k_0^2 - \alpha_n^2\right)^{1/2}, \tag{7}$$

here $A_n^{(m)\pm}$ are the unknown field amplitudes to be determined. All the incoming amplitudes should be zero, except the one, which corresponds to the incident field from the top. Therefore, in domain D_1, $A_n^{(1)+} = 0$, for all $n \neq 0$. In domain D_3, $A_n^{(3)-} = 0$ for all n.

The boundary conditions (4) can be implemented in a straight forward way to the recursive numerically stable S-matrix algorithm [14]. Thus, the solution for the field amplitudes $A_n^{(m)\pm}$ can be obtained.

To obtain the total reflectivity the z-component of the time-averaged Poynting vector should be analyzed:

$$\overline{S_z} = \frac{c}{8\pi}\mathrm{Re}\left[\vec{E} \times \vec{H}^*\right]_z = -\frac{c}{8\pi}\mathrm{Re}\left(E_y H_x^*\right), \tag{8}$$

Using E from (5) and $H_x = i(k_0)^{-1}\partial E/\partial z$ after averaging over x, we find the total reflectivity:

$$R = \sum_p \frac{\beta_p^{(1)}}{\beta_0^{(1)}} \left|A_p^{(1)-}\right|^2, \tag{9}$$

where the summation is carried over propagating orders in D_1.

The reflection of the grating for normal incidence is shown in Fig. 3(a). Five Fourier harmonics in the field decomposition (5) already

give the converged results. Four strong resonances with the reflection exactly equal to unity are observed in the region $0.5 < k_0/G < 1$ (black solid curve). This is the region, where three modes with $p = 0, \pm 1$ are propagating in the dielectric slab and only one zeroth mode in the air. Also cusp-like features in the reflection spectra are seen for $k_0/G > 1$, however, we will not focus on them. The observed resonant reflection is due to the excitation of the quasiguided modes in the slab. The frequencies of these modes in the absence of interface perturbation ($\gamma = 0$) are marked with red circles. Strictly speaking, for the perturbed interface ($\gamma > 0$), the eigenfrequencies of the structure are complex. However, for small perturbation $\gamma \ll 2\pi/k_0$, the eigenfrequencies should be close to those of the unperturbed slab, which are real. The analysis of complex eigenfrequencies for other structures will be carried in the next section.

If the small absorption term ε'' is introduced, all reflection resonances turn into absorption resonances, as shown by red curve in Fig. 3(a). This is due to the fact, that the quasiguided modes stay long enough in the structure to be strongly damped even in a weakly absorbing media. Fig. 3(b) shows the dependence of the absorption at resonance near $k_0/G = 0.5$ as a function of ε''. The first sharp peak at $\varepsilon''_{\max} = 0.007$ corresponds to resonant absorption on the quasiguided mode of the slab. Thus, we see that absorption

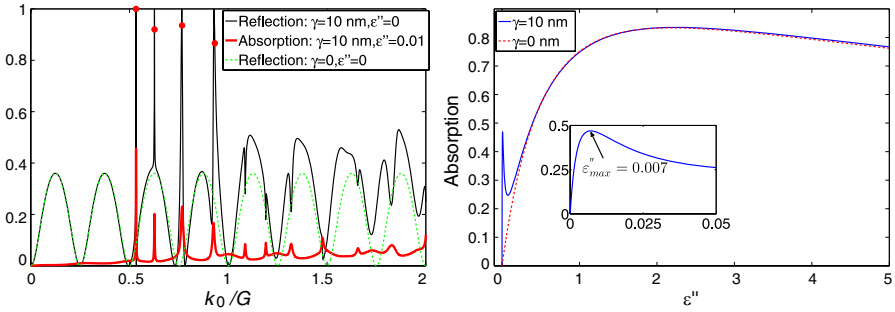

Figure 3. (a) Reflection of the structure, shown in Fig. 2. Green dashed and black solid curves correspond to the transparent unperturbed ($\gamma = 0$) and perturbed ($\gamma > 0$) slab, respectively. Waveguide modes of the unperturbed slab are marked with red circles. The red curve corresponds to the dielectric with small absorption term $\varepsilon'' = 0.01$. (b) Absorption at first resonance near $k_0/G = 0.5$ as a function of the loss term. The perturbed slab has an additional sharp absorption-based guided-mode resonance (AGMR).

peak experiences resonant behavior with respect to both frequency and material losses. After this resonance, as ε'' increases the absorption grows. This effect is due to the net attenuation of the field in the slab. At $\varepsilon'' = 2.25$ the absorption reaches its maximum value. In the limit of high ε'' the reflection tends to unity, due to high dielectric contrast with air. The absorption accordingly tends to zero. It should be noted that the change in the real part of permittivity $\varepsilon' \to \varepsilon' + \delta\varepsilon'$, where $\delta\varepsilon' = \varepsilon''_{\max}$ causes an extremely negligible shift (less than a linewidth) in the reflection spectra.

In the considered case, the AGMR peak is smaller than the broad one, corresponding to the net absorption, as seen in Fig. 3(b). However, in some cases, which are considered in the next section, this peak can be larger and even reach unity. This means that the introduction of small absorption ε'' can turn the incident radiation almost completely into heat.

Another peculiarity of the resonant reflection and absorption, is the extreme sensitivity with respect to the angle of incidence θ. Fig. 4(a) shows the angular dependence of the absorption for two of the peaks. One can see, both of the peaks split into two, as the angle increases. This can be understood from the dispersion diagram of the waveguide modes, which is shown in Fig. 4(b). The modes are doubly degenerate for normal incidence ($k_x = 0$), therefore, one absorption peak is observed. For the inclined incidence, the degeneracy is broken. Therefore, each of the peaks splits into two. Moreover, the second absorption peak experiences a significant increase in the magnitude for inclined incidence.

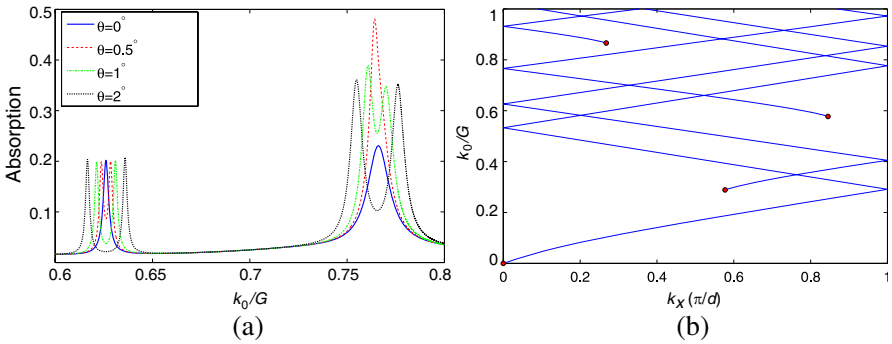

Figure 4. (a) Angular dependence of the absorption for the structure shown in Fig. 2, $\varepsilon'' = 0.01$. (b) Dispersion diagram of waveguide modes of the transparent unperturbed slab. The modes are doubly degenerate at $k_x = 0$.

3. NUMERICAL EXAMPLES FOR PERIODIC GRATINGS

The first structure to be analyzed is shown in Fig. 5. Sloping pyramids are arranged in a hexagonal lattice on top of the waveguide layer. The angle between the lateral face of the pyramid and the horizontal plane is $\alpha = 54.74^\circ$ (silicon etching angle). Constituent materials of the pyramids and of the waveguide layer are the same. Their permittivity is $\varepsilon = \varepsilon' + i\varepsilon''$, $\varepsilon' = 6.7$ shall be fixed, while ε'' is a variable parameter. The substrate is assumed to be infinite with permittivity $\varepsilon_s = 2.13$. The light is incident from the vacuum with the wave vector $\mathbf{k}$:

$$k_x = 0, \quad k_y = k_0 \sin\theta, \quad k_z = k_0 \cos\theta. \tag{10}$$

In this section, we consider normal light incidence $\theta = 0^\circ$ with electric field $\mathbf{E} = (0, E_y, 0)$.

The diffraction threshold frequencies into vacuum and substrate for the considered skewed lattice read:

$$f_{m_1,m_2} = \frac{c}{\sqrt{\varepsilon_{v,s}}} \frac{1}{d \sin\beta} \sqrt{m_1^2 + m_2^2 - 2m_1 m_2 \cos\beta},$$

where β is the angle between the lattice vectors (60° for a hexagonal unit cell), d is the length of the lattice vectors and $\{m_1, m_2\}$ are integers. The first diffraction order is opened at $f_{1,0} = 338.8\,\mathrm{THz}$ into the substrate.

In absence of the pyramids, and for lossless materials ($\varepsilon'' = 0$), the waveguide modes are purely guided and their eigenfrequencies are real. The lifetime of such modes is infinite and they cannot be excited by the light incident from vacuum. The periodic arrangement of the pyramids serves for coupling of the incoming light with the waveguide modes.

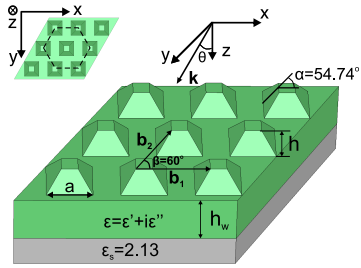

Figure 5. Pyramids arranged in a hexagonal lattice, translation vector $\mathbf{T} = m_1\mathbf{b_1} + m_2\mathbf{b_2}$, $|\mathbf{b_1}| = |\mathbf{b_2}| = d$, $m_{1,2} = 0, \pm1, \pm2, \ldots$. Structure parameters: $\varepsilon = \varepsilon' + i\varepsilon''$, $\varepsilon' = 6.7$, $\varepsilon_s = 2.13$, $d = 700\,\mathrm{nm}$, $h_w = 450\,\mathrm{nm}$, $h = 200\,\mathrm{nm}$, $a = 440\,\mathrm{nm}$, $\alpha = 54.74^\circ$, $\beta = 60^\circ$.

The eigenfrequencies become complex. Using the notation $\exp(-i\omega t)$, the eigenfrequencies have the form $\omega_1 - i\omega_2$, so that the fields decay in time domain $\sim \exp(-i\omega_1 t)\exp(-\omega_2 t)$.

The reflection spectrum of the structure is shown in Fig. 6(a). The frequency domain solver of CST Studio was used for the calculations. The strong features in the spectrum are due to the excitation of the quasiguided modes. Eight strong resonances, with reflection efficiency equal to unity are observed in the spectra below $f_{1,0} = 338.8\,\text{THz}$. Two of these resonances at $f = 221.8$ and $f = 290.5\,\text{THz}$ are extremely narrow, with line widths less than $0.1\,\text{THz}$. A sufficiently small frequency step must be chosen in order to detect them. Also two resonances, which manifest themselves as abrupt cusps in the reflection are located above $f_{1,0}$.

In order to confirm that the observed spectral features are in fact the manifestation of the quasiguided modes, we calculated the eigenvalues in COMSOL. Floquet-periodic boundary conditions were applied for the unit cell boundaries and scattering boundary conditions

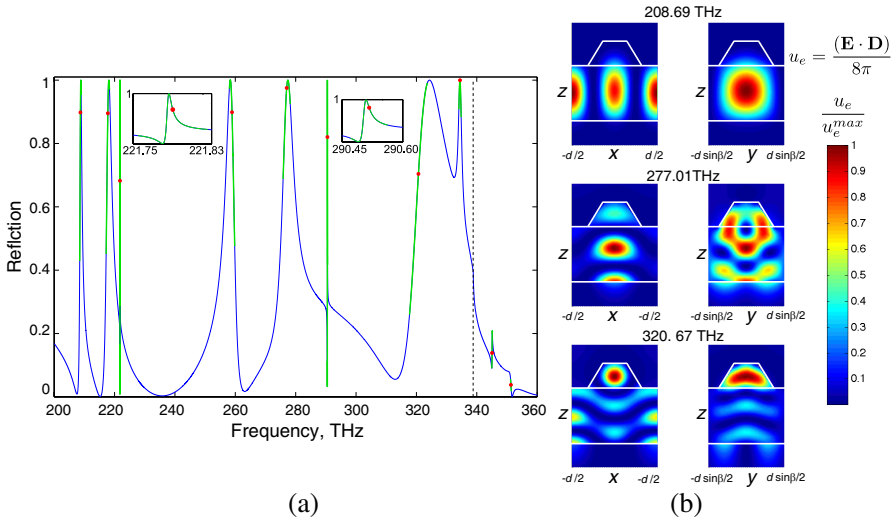

Figure 6. (a) Reflection of the structure, shown in Fig. 5, with $\varepsilon'' = 0$. Black dashed line corresponds to diffraction threshold at $f_{1,0} = 338.8\,\text{THz}$. Complex eigenfrequencies of the structure are listed in Table 1. Red circles correspond to the real part of the eigenfrequencies, imaginary part is highlighted with green. (b) Electric energy density (normalized) at three selected resonant frequencies. Left — Slice in the zx plane. Right — Slice in the zy.

for the upper and lower boundaries. From the obtained list of the eigenfrequencies we selected the modes with nonzero imaginary part (purely guided modes can not be excited by the incident plane wave and, therefore, do not manifest themselves in the spectra) and which are physically meaningful (according to the electric field distribution). These frequencies are listed in Table 1 and are also plotted in Fig. 6(a). As one can see, the real parts of the eigenfrequencies do not necessarily coincide with reflection maxima, but are rather close. The imaginary parts of the eigenfrequencies represent the inverse lifetime (or radiation losses) of the modes and should correlate with the resonance width. We highlighted the region between $\omega_1 - \omega_2/2$ and $\omega_1 + \omega_2/2$. A good correlation is clearly present.

Table 1. Complex eigenfrequencies of the structure, shown in Fig. 5.

Eigenfrequency, THz
$208.69 - 0.47i$
$217.77 - 1.12i$
$221.80 - 0.08i$
$258.91 - 1.78i$
$277.01 - 2.36i$
$290.52 - 0.09i$
$320.67 - 5.91i$
$334.43 - 0.77i$
$345.05 - 0.21i$
$351.31 - 0.27i$

Figure 6(b) shows the spatial distribution of the electric energy density at three selected resonances. As can be seen, high energy density can be concentrated in different regions of the structure. At frequency $f_1 = 208.69\,\text{THz}$ the energy density is high in the waveguide layer; at $f_2 = 277.01\,\text{THz}$ it is high in two regions — waveguide layer and pyramids; at $f_3 = 320.67\,\text{THz}$ energy density is high in the pyramids.

The absorption term ε'' plays a drastic role in spectra profile, due to AGMR effect. The absorption spectra of the structure for different ε'' values are shown in Fig. 7(a). The black solid curve corresponds to $\varepsilon'' = 0.005$. Now the absorption peaks coincide very well with the aforementioned eigenfrequencies. Because the perturbation $\varepsilon'' = 0.005$ is very small, it almost does not affect the eigenfrequency

values. Hence, resonant reflection/absorption peaks have almost the same width, and accordingly the same Q-factors, see also Appendix for the explanation. All resonances, even the narrow ones at $f = 221.8$ ($Q = 1150$) and $f = 290.5$ THz ($Q = 1475$) are clearly seen in the absorption spectra. The increase of the absorption up to the specific value $\varepsilon'' = 0.054$ causes several phenomena. Firstly, the resonances become wider. Narrow resonances at $f = 221.8$ and $f = 290.5$ THz are even smeared. Secondly, the resonances generally become stronger, except at $f = 290.5$ THz. The resonance at 334.4 THz, reaches an impressive value of almost 0.9. Further increase of ε'' makes the resonance less pronounced and at $\varepsilon'' = 0.6$ all the resonances are smeared.

The reflection spectra for the same ε'' values are shown in Fig. 7(b). The reflection at resonances accordingly decreases for the increasing ε'' values. It is remarkable that the reflection resonance at 334.4 THz (black dashed line) drops from unity to zero for specific value $\varepsilon'' = 0.054$. Ninety percents of the energy is absorbed and the rest is transmitted.

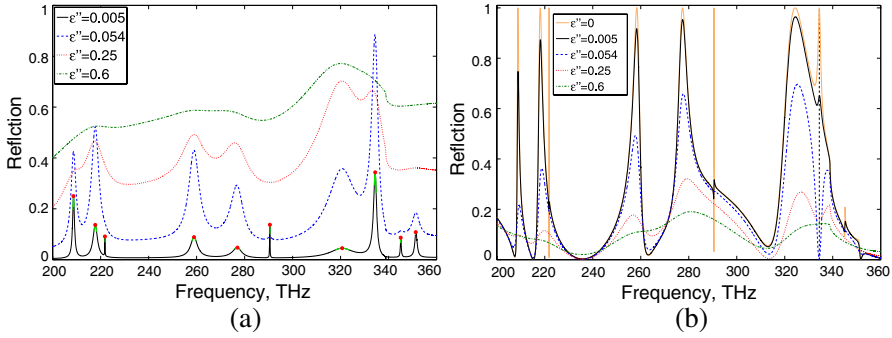

Figure 7. (a) Absorption spectra of the structure, shown in Fig. 5 for different absorption terms ε''. Red circles correspond to the real part of the eigenfrequencies (Table 1), imaginary part is highlighted with green. (b) Reflection spectra for the same values of ε''.

As demonstrated, high absorption can be observed even with extremely small losses. But it still remains of interest, if absorption can reach unity and, if full conversion of reflection to absorption is possible. In order to investigate that, we optimized a structure, which is shown in Fig. 8(a). We optimized five parameters to obtain maximum achievable conversion of the reflection to absorption at a

specified frequency 300 THz. Four parameters are geometrical (shown with double arrows) and one is the material absorption term ε''. For the obtained optimal parameters the absorption peak reaches unity (see black dash-dotted line in Fig. 8(b)), reflection is accordingly zero (see red dashed line). When no losses are present in the structure, the reflectivity at 300 THz is almost unity (blue solid curve). It is remarkable that such a small absorption term can almost fully convert reflection resonance into absorption.

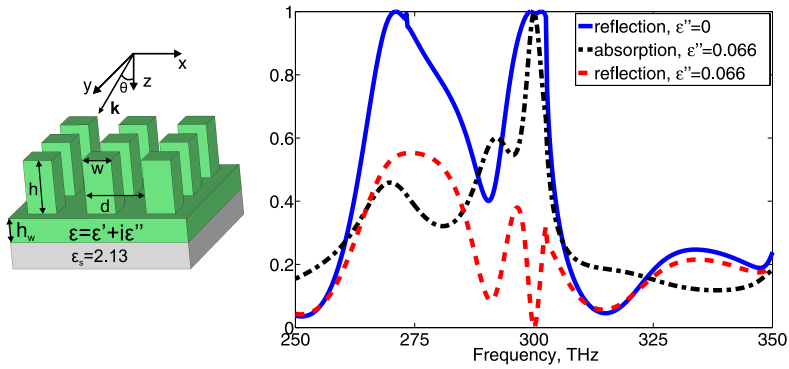

Figure 8. Bricks arranged in square lattice on top of the waveguide. Structure parameters: $\varepsilon = \varepsilon' + i\varepsilon''$, $\varepsilon' = 6.7$, $d = 680\,\text{nm}$, $h_w = 275\,\text{nm}$, $h = 610\,\text{nm}$, $w = 330\,\text{nm}$.

The AGMR effect allows to use a thermometer for sensing, instead of the optical detector scheme. If, for example, due to the interaction with some gas the material acquires nonzero ε'', the incident light will be strongly absorbed. This will lead to heating of the structure, which can be detected by simple temperature measurements. An example could be a hydrogen sensor, where the gasochromic coloration of WO_3 in the presence of hydrogen gas (H_2) [15] can be used.

Summarizing, we see two substantial benefits for sensors and switches to utilize the AGMR effect. Firstly, such sensors are highly sensitive. As seen, even extremely small losses lead to strong absorption peaks. The change of the real part of permittivity ε' requires a much more significant change for the observable shift of the reflection resonance. Secondly, the detecting scheme can be essentially simplified. Instead of measuring the optical response, the temperature of the structure can be measured.

4. STRUCTURES WITH THIN ABSORBING FILMS AND GRAPHENE MONOLAYERS

In the previous section we considered structures, where losses are distributed in the whole waveguide structure. However for sensor applications, structures with a thin layer that is in contact with the environment and changes its ε'', are more promising. Therefore, we examined cases of thin absorbing films in the structures.

Let us consider the structure, which is shown in Fig. 9(a). The only difference from the previous one (shown in Fig. 5), is that now merely a thin homogeneous layer $h = 50\,\text{nm}$ possesses losses, $\varepsilon''_a > 0$. Fig. 9(b) shows the absorption for different ε''_a values. For the sake of comparison, the black dashed line is reproduced from the structure with homogenously distributed losses. As one may see, the absorption in thin film is rather strong. Remarkable that at resonances $f = 221.8$ and $f = 290.5\,\text{THz}$ the absorption drops as losses increase. This behavior is not surprising, because each resonance reaches its maximum at some optimal value of ε''_a. This phenomenon was elucidated in Section 2 and demonstrated in Fig. 3(b). Moreover, the absorption in the film with $\varepsilon''_a = 0.005$ (red curve) is exceeding that of the homogenously distributed losses (black dashed line). Thus, reducing the absorption region can also promote an increase of absorption. Two resonances at $f = 221.8$ and $f = 290.5\,\text{THz}$ reach impressive Q-factors of 14000 and 7900, respectively. Due to small values of ε''_a, the positions

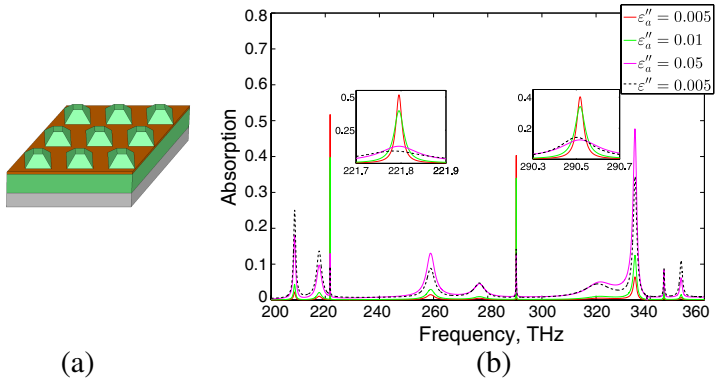

Figure 9. (a) structure equivalent in geometry to the one shown in Fig. 5. Losses are present only in the homogeneous region $h = 50\,\text{nm}$. (b) Absorption of the structure for different ε''_a values. Black dashed curve — absorption is present in the whole guiding block (reproduced from Fig. 7(a)).

of all resonances remain almost unaffected.

Exploring the realms of thin absorbing films in even further, we consider a monolayer of graphene [16]. This material is unique and has a number of remarkable properties [17], which can be used for sensor applications. The ability to change its conductivity in the presence of the external electric fields or to absorb hydrogen are two examples. The electrical conductivity of graphene in the visible spectral region was computed in [18]. The authors also calculated the reflection/transmission problem of the graphene sheet, embedded between dielectric media.

We consider a graphene monolayer in the structures, as shown in Fig. 10. The graphene monolayer can be taken into spectrum

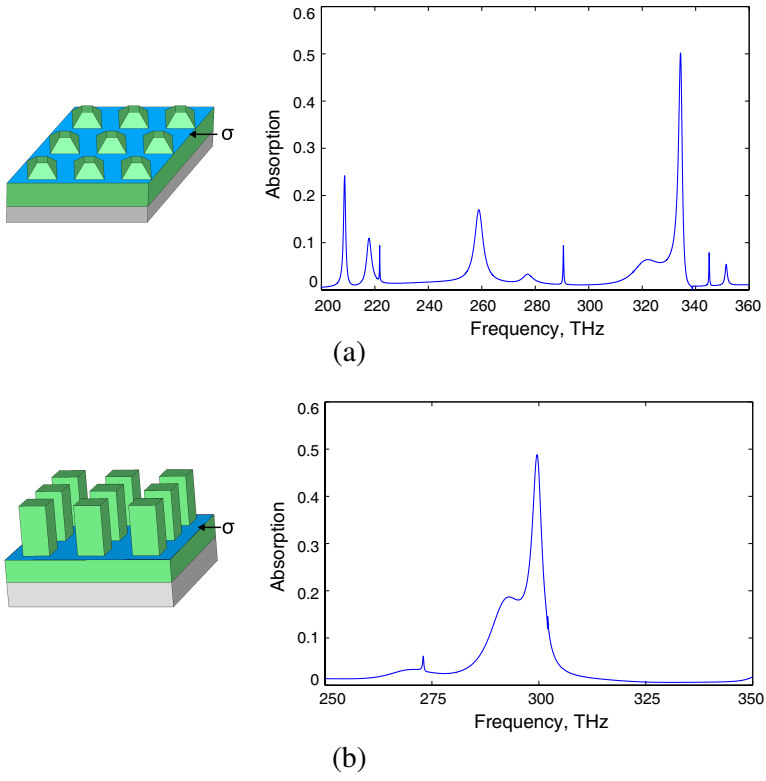

Figure 10. Absorption spectra of structures with a monolayer of graphene. Only graphene monolayer possess losses, the rest materials are transparent $\varepsilon'' = 0$. Structure (a) is equivalent to the one in Fig. 5, structure (b) is equivalent to Fig. 8.

calculations by means of the boundary conditions for the tangential components of the electric and magnetic fields:

$$\begin{cases} E_{y2} - E_{y1} = 0, \\ H_{x2} - H_{x1} = -\dfrac{4\pi}{c}\sigma E_{y1}, \\ E_{x2} - E_{x1} = 0, \\ H_{y2} - H_{y1} = \dfrac{4\pi}{c}\sigma E_{x1}, \end{cases}$$

where $\sigma(\omega)$ is the conductivity of graphene. In the considered frequency range, we assumed the graphene to be at half filling $\sigma(\omega) = \sigma_0 = \pi e^2/2h$ [18], where e is the electron charge and h is Planck's constant.

Calculated absorption spectra for two structures are shown in Fig. 10 on the right. Strong peaks correspond to the resonant absorption in the graphene monolayer. Note, that absorption in graphene monolayer without periodic gratings does not exceed 1.5% for same frequency range.

5. ANGULAR DEPENDENCE OF THE RESONANCES

In this section, we will briefly discuss the angular dependence of the resonances of the structures presented in Section 3. The components of the electric field are $\mathbf{E} = (0, E_y, E_z)$. Fig. 11 shows the absorption for normal and oblique incidences. As one can see, the spectra become more complicated and more absorption resonances appear, compared to normal incidence. For normal incidence some of the modes are

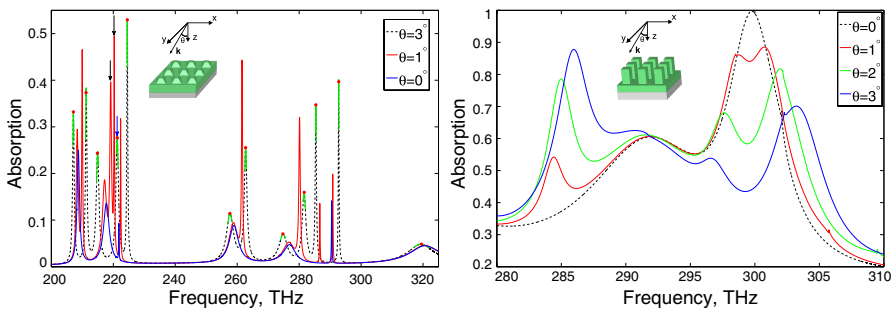

Figure 11. Angular dependence of the absorption of the structure, shown in (a) Fig. 5 with $\varepsilon'' = 0.005$. (b) Fig. 8(a) with $\varepsilon'' = 0.066$.

Table 2. Complex eigenfrequencies of the structure, shown in Fig. 5, $\theta = 3^\circ$, $\varepsilon'' = 0.005$.

Eigenfrequency, THz
$207.09 - 0.31i$
$211.20 - 0.28i$
$214.86 - 0.54i$
$221.29 - 0.51i$
$224.52 - 0.18i$
$257.64 - 1.39i$
$262.72 - 0.52i$
$274.76 - 1.56i$
$281.65 - 0.72i$
$285.39 - 0.23i$
$292.78 - 0.14i$
$319.54 - 5.08i$

inactive or degenerate due to symmetry properties. For the oblique incidence these states can become active and manifest themselves in the spectrum. In [5] the symmetry properties of the modes were analyzed to characterize optically active and inactive modes. Such detailed analysis is beyond the scope of this paper. As seen from Fig. 11(a), for $\theta = 1^\circ$ all of the absorption peaks split into two (except the broadest one near 320 THz). The spectral distance between these peaks increases, as the θ increases. Incidentally, the two peaks, which are marked with black arrows, approach each other and merge at $\theta = 3^\circ$. This merged peak is marked with a blue arrow.

The calculated eigenfrequencies of the first structure for the oblique incidence are listed in Table 2 and highlighted in Fig. 11(a). Very good correlation of the mode positions and linewidths with absorption peaks is observed. Noteworthy, that peak maxima reach impressively high values. For example, the peak at 224.5 THz exceeds 0.5, while the absorption outside of the resonance is below one percent.

6. CONCLUSIONS

It was shown that Absorption-Based Guided-Mode Resonances (AGMR) can be very sensitive with respect to small variations of losses. The absorption peaks observed experience a resonant behavior with respect to both frequency and material absorption. Q-factors of

AGMRs with small losses can be very high, approaching the values of the loss-free structures. It was demonstrated that total reflection can be turned into total absorption by means of introducing small losses. The position of the resonances remain almost unaffected, which can be advantageous for sensor and switch applications. Small variations of the imaginary part of permittivity have a much more pronounced impact on the optical response than the same variations of the real part. This feature opens opportunities to make sensors with high sensitivity. We suggest that this be used for a new kind of sensor for gas composition, pressure, biochemical composition, etc.. The only requirement is that the losses in the structure (or in its vicinity) are dynamically modified during the sensor operation. This can be achieved in a number of ways. An external electric field, for example, can modify the permittivity of some materials. This consequently, strongly affects the optical response. Such a situation can occur, for example, in graphene, where external fields change its conductivity.

As absorption resonances can reach impressive values, implying structure heating, the detection scheme can also be essentially simplified. Instead of utilizing an optical detector, simple temperature measurement of the structure can be performed. This offers additional opportunities such as cost reduction (in comparison with optical readout systems) and time averaged measurements. Extremely high angular sensitivity of the absorption/reflection peaks opens possibilities for the precise angle measurements.

ACKNOWLEDGMENT

The authors are very thankful to Alexander Dorodnyy from ETH Zürich for the discussions.

APPENDIX A.

In order to analyze the linewidth of the absorption peaks, let us consider the following problem. As in Section 2 the light is incident on a slab with a sinusoidal $\varepsilon(x)$ interface described by (1). For simplicity, the domain D_3 is now a perfect electric conductor (PEC), see Fig. A1. We take only $n = 3$ Fourier harmonics in the field decomposition of (5), and use the boundary conditions (4) (taking $\gamma = 10\,\text{nm}$, as in Section 2). This results in a system of linear equations with 9 unknown amplitudes. For the normally incident light the problem is symmetric and, therefore, the number of the unknown amplitudes reduces to 6.

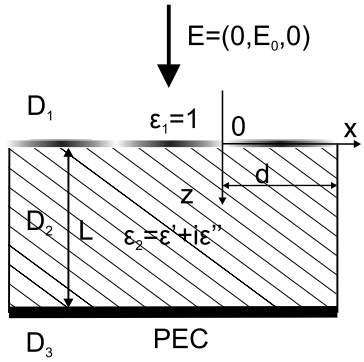

Figure A1. Dielectric grating with a sinusoidal $\varepsilon(x)$ interface at top and PEC at bottom. Permittivities are $\varepsilon_1 = 1$ and $\varepsilon_2 = \varepsilon' + i\varepsilon''$, $\varepsilon' = 4$. Thickness and period of the grating are $L = d = 100\,\text{nm}$. Light impinges normally on the structure.

Solving these equations for the absorption coefficient yields:

$$A = 1 - R = 1 - \left| \frac{B\left(\varepsilon'', \omega\right) - \mathbb{D}\left(\varepsilon'', \omega\right)}{\mathbb{D}\left(\varepsilon'', \omega\right)} \right|^2, \tag{A1}$$

here $B(\varepsilon'', \omega)$ is:

$$B\left(\varepsilon'', \omega\right) = -8\beta_0^{(1)} \sin\left(L\beta_0^{(2)}\right)\left(i\beta_1^{(2)} \cos\left(L\beta_1^{(2)}\right) + \beta_1^{(1)} \sin\left(L\beta_1^{(2)}\right)\right),$$

and $\mathbb{D}(\varepsilon'', \omega)$ is the determinant:

$$\begin{aligned}
\mathbb{D} \;=\; & -\exp(i\sigma_1)\left(\left(k_0^2\gamma\right)^2 + \left(\beta_0^{(1)} + \beta_0^{(2)}\right)\sigma_4\right) - \exp(-i\sigma_1)\left(\left(k_0^2\gamma\right)^2\right. \\
& \left. + \left(\beta_0^{(1)} - \beta_0^{(2)})\sigma_3\right) + 2\cos\sigma_2\left(\left(k_0^2\gamma\right)^2 + \beta_0^{(1)}\beta_1^{(1)} + \beta_0^{(2)}\beta_1^{(2)}\right)\right. \\
& -2i\sin\sigma_2\left(\beta_0^{(1)}\beta_1^{(2)} + \beta_1^{(1)}\beta_0^{(2)}\right), \\
\sigma_1 \;=\; & L\left(\beta_1^{(2)} - \beta_0^{(2)}\right), \qquad \sigma_2 = L\left(\beta_1^{(2)} + \beta_0^{(2)}\right), \\
\sigma_3 \;=\; & \left(\beta_1^{(1)} + \beta_1^{(2)}\right), \qquad \sigma_4 = \left(\beta_1^{(1)} - \beta_1^{(2)}\right),
\end{aligned}$$

where $\beta_n^{(m)}$ are defined in (7). Considering ε'' as a small parameter, we can expand both numerator and denominator of (A1), keeping only linear terms:

$$\begin{aligned}
A \;&\approx\; 1 - \left| \frac{B_1(\varepsilon'', \omega) - \mathbb{D}_1(\varepsilon'', \omega)}{\mathbb{D}_1(\varepsilon'', \omega)} \right|^2, \qquad \text{(A2)} \\
B_1(\varepsilon'', \omega) \;&=\; B^{(0)}(\omega) + B^{(1)}(\omega)\varepsilon'', \\
\mathbb{D}_1(\varepsilon'', \omega) \;&=\; \mathbb{D}^{(0)}(\omega) + \mathbb{D}^{(1)}(\omega)\varepsilon''.
\end{aligned}$$

The principal term to be kept in the numerator of (A2) is $\mathbb{D}^{(0)}(\omega)$, therefore, the expression simplifies to:

$$A \approx 1 - \left| \frac{\mathbb{D}^{(0)}(\omega)}{\mathbb{D}_1(\varepsilon'', \omega)} \right|^2. \tag{A3}$$

As seen from Fig. A2(a), for small value of ε'' the expansion (A2) is a very good approximation of (A1). The simplified expression (A3) describes the absorption spectrum appropriately.

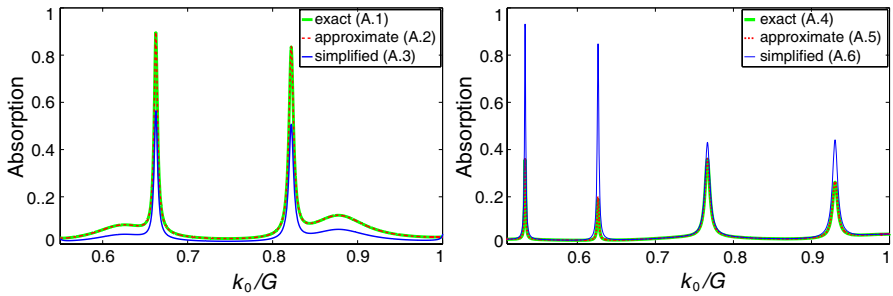

Figure A2. Absorption spectra of the structure shown in (a) Fig. A1 and (b) Fig. 2; $\gamma = 10\,\text{nm}$, $\varepsilon'' = 0.01$. Green solid lines correspond to the exact solutions, red dashed lines — approximate solutions, blue solid lines — simplified expression.

When $\varepsilon'' = 0$, the numerator and denominator of (A3) are equal, yielding zero absorption and unity reflection, respectively. The function $\mathbb{D}^{(0)}(\omega)$ is zero for the complex eigenfrequency $\omega_0 = \omega_1 - i\omega_2$, $\mathbb{D}^{(0)}(\omega_0) = 0$. For the real part of the eigenfrequency ω_1, $\mathbb{D}^{(0)}(\omega_1)$ exhibits a minimum and becomes noticeably smaller than $\mathbb{D}_1(\varepsilon'', \omega_1)$, if $\varepsilon'' > 0$. Thus, strong increase of absorption at resonant frequency ω_1 is observed. The width of the absorption peak is correlated with the width of denominator $\mathbb{D}_1(\varepsilon'', \omega)$ and, hence, with the imaginary part of the eigenfrequency ω_2. Which grows as losses increase $\omega_2(\varepsilon_2'') > \omega_2(\varepsilon_1'')$, $\varepsilon_2'' > \varepsilon_1''$.

Let us now come back to the problem of light reflection from a dielectric slab, shown in Fig. 2. Expression for the absorption has the same form as (A1), with the only difference that the transmission should also be taken into account:

$$A = 1 - R - T = 1 - \left| \frac{B(\varepsilon'', \omega) - \mathbb{D}(\varepsilon'', \omega)}{\mathbb{D}(\varepsilon'', \omega)} \right|^2 - \left| \frac{C(\varepsilon'', \omega)}{\mathbb{D}(\varepsilon'', \omega)} \right|^2, \tag{A4}$$

here $B(\varepsilon'', \omega)$, $C(\varepsilon'', \omega)$ and $\mathbb{D}(\varepsilon'', \omega)$ are some cumbersome analytical expressions. Performing the same expanding and simplification

procedure as in (A2) and (A3), we obtain:

$$A \approx 1 - \left| \frac{B_1(\varepsilon'', \omega) - \mathbb{D}_1(\varepsilon'', \omega)}{\mathbb{D}_1(\varepsilon'', \omega)} \right|^2 - \left| \frac{C_1(\varepsilon'', \omega)}{\mathbb{D}_1(\varepsilon'', \omega)} \right|^2, \quad \text{(A5)}$$

$$A \approx 1 - \left| \frac{\mathbb{D}^{(0)}(\omega)}{\mathbb{D}_1(\varepsilon'', \omega)} \right|^2. \quad \text{(A6)}$$

As can be seen from Fig. A2(b) the approximation (A5) is in very good agreement with the exact solution (A4) and the absorption peaks are well reproduced by the simplified formula (A6). The line width of the absorption peak is correlated with the width of the determinant $\mathbb{D}_1(\varepsilon'', \omega)$, while the width of the resonant reflection peak for the loss-free case is correlated with the width of $\mathbb{D}^{(0)}(\omega)$. Since $|\mathbb{D}_1(\varepsilon'', \omega)| > |\mathbb{D}^{(0)}(\omega)|$, the resonant absorption peak is wider than that of the resonant reflection, however in the limit of small ε'' the difference becomes negligible.

It should be noted, that the line shape of the resonant reflection peaks is strongly asymmetric, in contrast to that of the resonant absorption (see, for example, Fig. 7). Therefore, it is not easy to give a precise definition of the line width for the reflection peak. Using the definition of Full Width at Half Maximum (FWHM), it can appear that absorption peaks are, actually, narrower than the peaks of reflection. Especially in cases when the resonances are located close to each other. As an example, using FWHM definition, the absorption peak at $f = 334.43\,\mathrm{THz}$ in Fig. 7(a) for $\varepsilon'' = 0.005$ is obviously narrower than the reflection peak in Fig. 7(b) for $\varepsilon'' = 0$.

REFERENCES

1. Wang, S. S. and R. Magnusson, "Theory and applications of guidedmode resonance filters," *Applied Optics*, Vol. 32, No. 14, 2606–2613, 1993.
2. Gale, M. T., K. Knop, and R. Morf, "Zero-order diffractive microstructures for security applications," *SPIE Conference on Optical Security and Anticounterfeiting Systems*, 83–89, 1990.
3. Liu, Z. S., S. Tibuleac, D. Shin, P. P. Young, and R. Magnusson, "High-efficiency guided-mode resonance filter," *Optics Letters*, Vol. 23, No. 19, 1556–1558, 1998.
4. Pottage, J. M., E. Silvestre, and P. St. J. Russell, "Vertical-cavity surface-emitting resonances in photonic crystal films," *JOSA A*, Vol. 18, No. 2, 442–447, 2001.
5. Tikhodeev, S. G., A. L. Yablonskii, E. A. Muljarov, N. A. Gippius, and T. Ishihara, "Quasiguided modes and optical properties of

photonic crystal slabs," *Physical Review B*, Vol. 66, No. 4, 045102, 2002.

6. Magnusson, R., D. Wawro, S. Zimmerman, and Y. Ding, "Resonant photonic biosensors with polarization-based multiparametric discrimination in each channel," *Sensors*, Vol. 11, No. 2, 1476–1488, 2011.
7. Cunningham, B. T., J. Pepper, B. Lin, P. Li, J. Qiu, and H. Pien, "Guided mode resonant filter biosensor using a linear grating surface structure," US Patent 7,070,987, Jul. 4, 2006.
8. Lee, K. J., D. Wawro, P. S. Priambodo, and R. Magnusson, "Agarose-gel based guided-mode resonance humidity sensor," *IEEE Sensors Journal*, Vol. 7, No. 3, 409–414, 2007.
9. Foland, S., K. H. Choi, and J. B. Lee, "Pressure-tunable guided-mode resonance sensor for single-wavelength char acterization," *Optics Letters*, Vol. 35, No. 23, 3871–3873, 2010.
10. Fattal, D. A., A. Pyayt, R. G. Beausoleil, and W. Wu, "Angle sensor, system and method employing guided-mode resonance," US Patent App. 12/864,234, Mar. 4, 2008.
11. Magnusson, R., "Guided-mode resonance sensors employing angular, spectral modal, and polarization diversity for highprecision sensing in compact formats," WO Patent WO/2008/031,071, Mar. 13, 2008.
12. Komarevskiy, N., V. Shklover, L. Braginsky, and C. Hafner, "Absorption based guided-mode resonance sensor/switch and method for sensing physical changes in various environments," 2012PA00021EP, Oct. 10, 2012.
13. Braginsky, L. and V. Shklover, "Light propagation in an imperfect photonic crystal," *Physical Review B*, Vol. 73, No. 8, 085107, 2006.
14. Li, L., "Formulation and comparison of two recursive matrix algorithms for modeling layered diffraction gratings," *Journal of the Optical Society of America*, Vol. 13, 1024–1035, 1996.
15. Georg, A., W. Graf, R. Neumann, and V. Wittwer, "Mechanism of the gasochromic coloration of porous WO3 films," *Solid State Ionics*, Vol. 127, No. 3, 319–328, 2000.
16. Geim, A. K. and K. S. Novoselov, "The rise of graphene," *Nature Materials*, Vol. 6, No. 3, 183–191, 2007.
17. Geim, A. K., "Graphene: Status and prospects," *Science*, Vol. 324, No. 5934, 1530–1534, 2009.
18. Stauber, T., N. M. R. Peres, and A. K. Geim, "The optical conductivity of graphene in the visible region of the spectrum," Arxiv preprint arXiv: 0803.1802, 2008.